Author(s): Julin, Juhani; Chaudhuri, Saumyadip; Laitinen, Mikko; Sajavaara, Timo; Maasilta, Ilari

Title: Stability, sub-gap current, 1/f-noise, and elemental depth profiling of annealed Al:Mn-AlOX-Al normal metal-insulator-superconducting tunnel junctions

Year: 2016

Version:

Please cite the original version:

Julin, J., Chaudhuri, S., Laitinen, M., Sajavaara, T., & Maasilta, I. (2016). Stability, sub-gap current, 1/f-noise, and elemental depth profiling of annealed Al:Mn-AlOX-Al normal metal-insulator-superconducting tunnel junctions. AIP Advances, 6(12), Article 125026. https://doi.org/10.1063/1.4972205

Stability, sub-gap current, 1/f-noise, and elemental depth profiling of annealed Al:Mn-AlO_X-Al normal metal-insulator-superconducting tunnel junctions

J. K. Julin, S. Chaudhuri, M. Laitinen, T. Sajavaara, and I. J. Maasilta

Citation: AIP Advances **6**, 125026 (2016); doi: 10.1063/1.4972205
View online: http://dx.doi.org/10.1063/1.4972205
View Table of Contents: http://aip.scitation.org/toc/adv/6/12
Published by the American Institute of Physics

Stability, sub-gap current, 1/f-noise, and elemental depth profiling of annealed Al:Mn-AlO_x-Al normal metal-insulator-superconducting tunnel junctions

J. K. Julin,[1] S. Chaudhuri,[1,a] M. Laitinen,[2] T. Sajavaara,[2] and I. J. Maasilta[1,b]
[1]*Nanoscience Center, Department of Physics, University of Jyvaskyla, P.O. Box 35, FI-40014 Jyvaskyla, Finland*
[2]*Accelerator Laboratory, Department of Physics, University of Jyvaskyla, P.O. Box 35, FI-40014 Jyvaskyla, Finland*

(Received 23 September 2016; accepted 30 November 2016; published online 15 December 2016)

In this paper we report a study of the effect of vacuum annealing at 400°C on the properties of normal metal-insulator-superconductor (NIS) tunnel junctions, with manganese doped aluminium (Al:Mn) as the normal metal, aluminum as the superconductor and amorphous aluminum oxide as the tunneling barrier (Al:Mn-AlO_x-Al). The annealing treatment improves the stability of the junctions, increases their tunneling resistance and does not have a negative impact on the low-temperature current-voltage characteristics. The measured $1/f$ resistance noise of the junctions also changes after annealing, in the best case decreasing by over an order of magnitude. All these observations show that annealing is a viable route to improve NIS junction devices after the sample has been fabricated. [http://dx.doi.org/10.1063/1.4972205]

I. INTRODUCTION

Superconducting tunnel junctions are important components for applications in quantum information processing,[1] metrological applications,[2] solid state coolers,[3] ultrasensitive radiation detection[4] and low-temperature thermometry.[5] In addition, normal state junctions also find applications as ultrasensitive electrometers and charge pumps in single electron transistor (SET) devices.[2,6] Just like for any other electronic components, it is desirable to fabricate tunnel junction devices whose characteristics are reproducible, stable and exhibit minimal aging effects. Unfortunately, many fabrication protocols do not automatically guarantee this, but special measures such as vacuum annealing,[7] agressive cleaning[8] and multistep oxidation[9] have been shown to improve the stability of Al-AlO_x-Al tunnel junctions.

Another quite general problem is that many electronic devices exhibit excess non-equilibrium noise which typically has a frequency spectrum close to $1/f$.[10,11] In superconducting tunnel junctions, $1/f$ noise has been observed both in the critical current and the junction resistance of the devices,[12–19] typically interpreted as arising from trapping and detrapping of charges in the amorphous tunnel barrier material AlO_x, leading to fluctuations in the effective junction area.[16,19,20] This junction resistance and critical current noise can eventually become a limiting factor for the coherence of superconducting quantum bits.[1,16] Thus, it is interesting that the same vacuum annealing treatments that stabilize and improve the DC characteristics of Al-AlO_x-Al tunnel junctions also lead to the reduction of the $1/f$ junction resistance noise.[13] In SET devices and charge qubits, however, the $1/f$ noise is typically dominated by charge noise that may also originate from the surroundings of the junctions, and not only the barrier.[21–25] For that reason, vacuum annealing may not be as effective for single electron devices, although detailed studies are lacking.

[a]Current address: Picodeon Ltd Oy, Piisilta 1, FI-91100 Ii, Finland.
[b]Electronic mail: maasilta@jyu.fi

Our previous annealing work[7,13] focused only on Al-AlO_x-Al junctions, which are applied either as superconducting quantum bits or radiation detectors in the SIS (superconductor-insulator-superconductor) geometry, or as single electron devices when in the normal state. However, many other applications actually require NIS (normal metal-insulator- superconductor) junctions, where one of the electrodes is in the normal state while the other is superconducting. This means that the junctions have to be fabricated using two different materials, with most common combinations being Cu-AlO_x-Al, AuPd-AlO_x-Al (AuPd alloy) and Al:Mn-AlO_x-Al (Al with Mn impurities).[2,5] For the above reason, the question we decided to address in this paper is: How does the vacuum annealing treatment affect the properties of NIS junctions? If stability, sub-gap current or $1/f$ noise can be improved, one could perhaps improve the performance of hybrid single electron SINIS turnstiles,[2,26] SINIS thermometers and coolers and NIS-junction based radiation detection.[27–29] In particular, the cooling performance of a non-ideal NIS junction is very sensitive to the level of sub-gap current,[30,31] typically parametrized by the broadening of the superconducting quasiparticle density of states (DOS).[32] Excess sub-gap current can also lead to errors in pumping in SINIS turnstiles.[2]

Here, we present results on the effects of vacuum annealing on NIS junctions, concentrating on manganese-doped aluminum (Al:Mn) as the normal metal material of the NIS junctions.[33–36] We find that vacuum annealing at 400 °C improves the stability of the junctions, increases the tunneling resistance, and has no negative effects on the sub-gap current. The $1/f$ resistance noise decreases in most cases, but, this effect is sensitive to the pre-annealing junction quality. Finally, we present elemental depth profiling results on junctions before and after annealing, showing that some, but not all impurities are affected by the annealing. A non-uniform manganese profile shows a reorganization after annealing.

II. SAMPLE FABRICATION

All NIS tunnel junction devices were fabricated on oxidized silicon chips using electron-beam lithography and two-angle electron-beam evaporation in a single lithography step, shown schematically in Fig. 1(a), in three different evaporators. All of these evaporators rely on the same electron-beam heating operation, but differ on the level of vacuum, source-sample distance and usage. The junction size was kept constant at around 200 nm × 300 nm, and the metal layer thicknesses were 50-70 nm for the superconducting Al layer, and ranged from ∼30 nm to ∼150 nm for the normal metal layer. The tunneling barrier was formed by *in-situ* oxidization of the aluminum surface in an atmosphere of pure oxygen (pressure ∼ 50 mbar) for 4 minutes at room temperature. A scanning electron micrograph of a typical junction is shown in Fig. 1(b).

As it has been found before that resist residues can be detrimental to the junction quality,[7,8] the chip was always cleaned after the resist development but prior to the metal deposition with an O_2 plasma. The plasma cleaning was performed in a reactive ion etcher at 30-40 W power and with a pressure of 40 mtorr and 50 sccm flow rate. After the depositions, a post-oxidation was also performed to protect the junctions. For the normal metal, we used several materials - copper, gold, silver, gold-palladium alloy and finally Al:Mn, where the source had nominally 2 atomic % of Mn. The deposition rates were always in the range 1-3 Å / s.

All copper, gold, and silver NIS junctions and some aluminum SIS junctions were fabricated in the ultra-high vacuum (UHV) evaporator with pressure during evaporation around $\sim 10^{-8}$ mbar. We have seen before that junctions fabricated in this particular evaporator are of good quality.[7,37] The aluminum-manganese and gold-palladium junctions, on the other hand, were fabricated in two different high-vacuum ($\sim 10^{-5}$ mbar) evaporators, Edwards Auto 306 and Balzers Baltec BAE 250. We call these two evaporators HV1 and HV2, respectively, from now on. The main usage difference between them is that HV1 was exclusively used for this project during the study, whereas HV2 is in general in heavy use with many different materials being evaporated. Thus, the expectation is that HV1 will produce slightly higher quality tunnel junctions. Another difference is that in HV1, the electron beam is swept in the crucible, producing a larger hot spot than in HV2, where the e-beam is stationary.

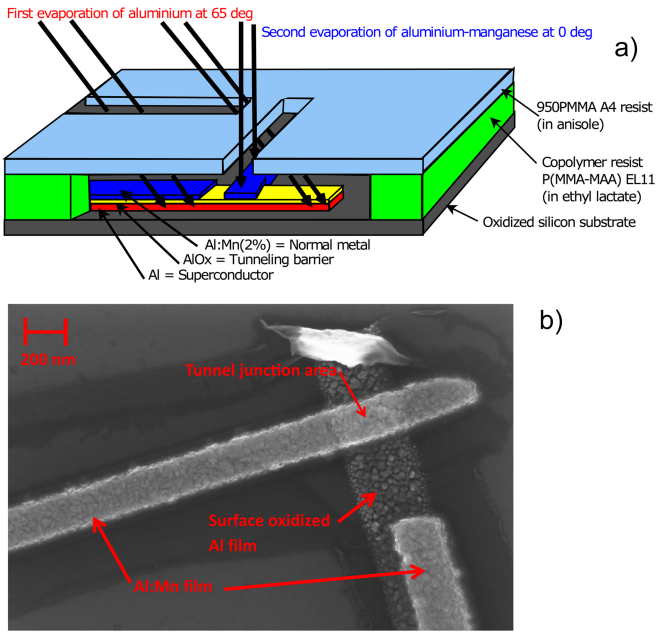

FIG. 1. (a) A Schematic of the sample fabrication process using two-angle evaporation of metals. Electron beam lithography was used to expose a dual layer resist (PMMA and co-polymer), with the developed openings allowing the metals to reach the surface of the silicon chip. In-situ oxidation of the aluminium film grows the tunneling barrier between the two metal depositions. (b) A scanning electron microscope image of a typical Al:Mn-AlO_x-Al NIS tunnel junction.

III. ANNEALING TREATMENT AND AGING

Previously, we observed that Al-AlO_x-Al tunnel junction device parameters such as charging energy, tunneling resistance R_T, barrier thickness and height increased after a vacuum annealing treatment,[7] while the superconducting gap value remained unchanged. In addition, the $1/f$ resistance noise was lowered, in some cases by an order of magnitude.[13] The main goal of this work is to study the behavior of these observables for NIS junctions after vacuum annealing. However, another parameter of paramount importance for NIS tunnel junction applications is the level of sub-gap current, often parametrized by the effective broadening of the superconducting density of states, the Dynes parameter.[5,32] Note that this parameter can describe several physical processes: genuine sub-gap states caused by a finite lifetime of the quasiparticles,[32] photon-assisted tunneling due to environmental noise[38] or higher-order two-particle (Andreev) tunneling.[39–41] To our knowledge, the influence of annealing on the sub-gap current in NIS junctions was not studied before.

For annealing, the samples were mounted on a stage and inserted into a tubular boron nitride resistive heating element (maximum temperature 600°C) located in a high vacuum chamber. The temperature of the sample stage was constantly monitored, and upon reaching the desired annealing temperature[7] of 400°C the stage was pulled out and left in vacuum for slow cooling down, so the cooling time back to room temperature was about 4 hours. The annealing protocol used was the same as what was used for Al-AlO_x-Al junctions.[7,13]

Unfortunately, the annealing of the copper, gold, silver or gold-palladium normal metal NIS junctions never produced good results. Copper, gold and gold-palladium based devices typically suffered from serious decrease of R_T after annealing, in contrast to the increase seen for Al. For some junctions we checked that this remaining resistance was not due to tunneling by observing that the resistance decreased with lowering temperature (an increase happens for tunnel junctions). Strong morphological changes of the Cu films were also visible. Silver, on the other hand, typically suffered from open circuits after annealing, and even in some of the non-annealed samples.

The only NIS junctions that ever produced consistently good results in the annealing were aluminum-manganese Al:Mn-AlO_x-Al junctions. We have statistics from 125 junctions with typical pre-annealing tunneling resistances in the range R_T=10 – 100 kΩ (specific junction resistances R_TA

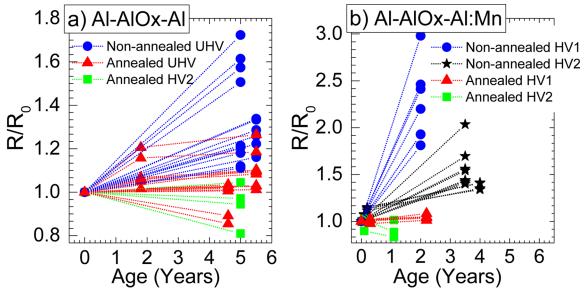

FIG. 2. Measured room temperature tunneling resistance change R/R_0 where R_0 is the tunneling resistance at time zero, as a function of time for a) Al-AlOx-Al and b) Al:Mn-AlOx-Al samples fabricated in UHV, HV1 and HV2 evaporators with and without annealing. Here the aging of non-annealed samples is strong, although not that pronounced for UHV-fabricated Al-AlOx-Al samples. Annealing reduces the aging in all samples.

$\sim 600 - 6000\Omega(\mu m)^2$), fabricated with both evaporators HV1 and HV2. The tunneling resistance of the junctions always increased after annealing, on the average by 80 % for HV1 and by 400 % for HV2, but the increase was quite variable from junction to junction. These results are consistent with the earlier results for Al-AlO_x-Al junctions that were only fabricated in HV2 in Ref. 7. We do not have direct evidence what causes this increase, but point out that transmission electron microscopy results on annealing of magnetic tunnel junctions with AlOx barriers[42] have shown homogenization of the tunneling barrier, which could explain the increase as the thinnest barrier regions dominating conductance[40,43] are removed.

For a number of both Al-AlO_x-Al and Al:Mn-AlO_x-Al junctions, we also studied the stabilization properties of the junctions after annealing, for some junctions for over five years, with some representative data shown in Fig. 2. The samples were kept in room air for the whole duration of the stability study. First of all, we see from Fig. 2 that some long term drift in R_T is still observable even in the annealed Al-AlO_x-Al junctions, but maximally only ±20% over five years. Some individual junctions remained stable even within 2 %. Non-annealed Al-AlO_x-Al junctions fabricated in UHV conditions showed a much larger spread of R_T increase, between 20 - 70 % in five years.

In contrast, the non-annealed Al:Mn-AlO_x-Al junctions increased their R_T by much larger factors, between 30 % to even 300 % in just two years. This larger aging compared to non-annealed Al-AlO_x-Al junctions can perhaps be attributed to the worse vacuum conditions of the HV1 and HV2 evaporators, producing extra defects in the barrier.[7] Curiously, within the set of Al:Mn-AlO_x-Al samples, the HV1 samples seemed to age faster, even though the HV1 evaporator is considered to be slightly cleaner. After annealing, the aging is again much reduced, to approximately ±10% in 1-2 years, roughly in agreement with the Al-AlO_x-Al samples. Interestingly, aging by resistance decrease was also detected in some annealed samples. The reason for the decrease is currently unknown.

IV. ELECTRICAL CHARACTERIZATION OF THE AL:MN-ALO$_x$-AL NIS JUNCTIONS

For some of the Al:Mn-AlO_x-Al NIS junctions, low-temperature current-voltage (I-V) measurements were carried out using a He3-He4 dilution refrigerator both before and after annealing. The DC current and voltage were measured with Ithaco 1201 voltage and 1211 current preamplifiers, respectively. The measurement lines in the refrigerator had three different stages of filtering: discrete pi-filters at 4 K, RC-filters at base temperature ~ 0.1 K, and, finally, microwave filtering between the two discrete filter blocks by Thermocoax cables of length 1.5 m. These filters are typically important in the low-temperature measurements of NIS junctions, as they cut off a large portion of the environmental noise power that could overheat the junctions or cause excess photon-assisted tunneling.[38] However, we point out that even stronger filtering and shielding measures[38,44,45] are necessary for some experiments, such as SINIS single-electron charging[46,47] or qubit[44,45] experiments.

Fig. 3 shows examples of measured low-temperature ($T \sim 0.15$ K) I-V characteristics of typical junctions, fabricated either in evaporator HV1 [Fig. 3 (a)] or in evaporator HV2 [Fig. 3(b)], both before and after annealing. The results in b) for HV2 are from physically the same junction before

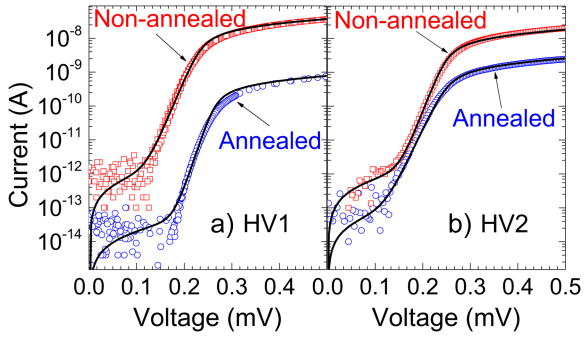

FIG. 3. Current-voltage characteristics of Al:Mn-AlO_x-Al NIS junctions fabricated in evaporator a) HV1 and b) HV2, measured at 120-160 mK both before and after annealing. The open symbols denote the measured response, while the lines are the corresponding theoretical fits. Fitting to theory results in a gap $\Delta \sim 0.25$ meV and a Dynes parameter $\Gamma/\Delta \sim 1 \times 10^{-4}$ for all four curves. In b), the R_T changed from 24 kΩ to 170 kΩ after annealing.

and after annealing, whereas in a) the samples are from the same chip, but are different individuals. The logarithmic current axis used in Fig. 3 allows the identification of the small sub-gap current component more easily. In addition to the measured data, the plots also show theoretical fits based on the standard single-particle tunneling model $I = \frac{1}{2eR_T}\int_{-\infty}^{\infty} d\epsilon N_S(\epsilon)(f_N(\epsilon - eV) - f_N(\epsilon + eV))$, where $f_N(\epsilon)$ is the Fermi function in the normal metal electrode, and $N_S(\epsilon)$ is the normalized broadened superconducting quasiparticle DOS in the Dynes model:[32] $N_S(\epsilon, T_S) = \left|\mathrm{Re}\left(\frac{\epsilon+i\Gamma}{\sqrt{(\epsilon+i\Gamma)^2-\Delta^2}}\right)\right|$, with Γ the broadening (Dynes) parameter and Δ the superconducting gap.

The conclusions from the $I - V$ measurements are quite clear: First of all, the theory fits the experiments perfectly well both before and after annealing. Second, neither the superconducting gap Δ nor the effective broadening Γ change after the annealing. All changes are reflected in the increase of R_T which includes the influence of all the tunnel barrier parameters for single particle tunneling. The gap insensitivity is consistent with our earlier results with Al-AlO_x-Al junctions. The value of the Dynes parameter and thus the value of sub-gap current is also consistent with earlier measurements using non-annealed Cu-AlO_x-Al junctions measured in the same refrigerator.[37] Clearly, annealing has no negative effects on the superconducting properties.

It would, of course, have been extremely interesting if we could have seen a reduction of Γ. On one hand, it has been shown by other groups that Γ for Al-based NIS junctions is typically limited by environmentally induced photon assisted tunneling[38] for junctions of low barrier transparency such as ours here. A significant reduction of Γ by annealing is not expected in that case (some effect could arise due to the change of R_T and thus change in impedance matching). On the other hand, if our broadened DOS is simply modeling higher order, Andreev tunneling, then we would expect that the sub-gap current should decrease even relative to the current above the gap, as the rates of second order processes scale as[40,48,49] $1/R_T^2$. Thus the fact that Γ stays constant seems to indicate that the sub-gap current in our junctions and setup is most likely dominated by the first option.

Let us, nevertheless, comment on the possible significance of annealing on the sub-gap current in the case where Andreev current is dominating. This is interesting, because Andreev processes are currently the main source of errors in SINIS hybrid turnstiles,[2] and they lead to parasitic heating in NIS coolers.[39] It was already demonstrated in Ref. 43 that due to the $1/R_T^2$ dependence, Andreev sub-gap current is sensitive to the fluctuations of the tunnel barrier properties. It was also shown that for typical non-annealed junctions, the barrier fluctuations can increase the Andreev current by a large factor ~ 60, based on the barrier thickness variations observed with TEM imaging.[43] Thus, if the barrier becomes more uniform after annealing as has been seen in some cases,[42] strong improvements in the suppression of Andreev-current are expected.

V. ELECTRICAL CHARACTERIZATION OF 1/*f* NOISE

We also studied the effect of annealing on $1/f$ noise properties of Al:Mn-AlO_x-Al NIS junctions. In the noise measurements, two junctions fabricated at the same time on the same chip are connected in series, with a base electrode between them, to allow for a bridge-type measurement,[13,50] schematically shown in figure 4. The operational principle of the setup is the following: The resistance noise from the tunnel junctions is first modulated using an ac excitation around 1 kHz, measured using pre-amplifiers (Ithaco 1201) for each junction, and then demodulated back to the original frequency range using lock-in amplifiers (Stanford Research Systems SR830). Finally, the noise spectrum is recorded using a two-channel spectrum analyzer (Agilent 89410A) operated in the cross-correlation mode. By balancing the bridge with the adjustable ballast resistor, the excitation is not measured directly, only noise. This bridge setup completely eliminates the problem of the low frequency $1/f$ noise from the voltage preamplifiers, by shifting the measured junction noise band into the lowest noise frequency region for the preamplifiers, typically around 1 kHz.

Representative results of the $1/f$ resistance noise measurements at room temperature for Al:Mn-AlO_x-Al samples (fabricated in both evaporators HV1 and HV2) are shown in Fig. 5(a) and 5(b), both before and after annealing. For comparison, we also show the earlier results[13] for the Al-AlO_x-Al junctions in Fig. 5(c). The results are plotted as spectral density S_R divided by the total double junction resistance squared R_T^2 so that the effect of varying R_T is scaled out.

First, by comparing the non-annealed results, we see that the scaled $1/f$ noise level for Al:Mn-AlO_x-Al junctions is generally speaking in the same order of magnitude as for the UHV fabricated non-annealed Al-AlO_x-Al junctions. This is logical, if the source of the noise is the same, as the barrier material is still the same. It is curious, though, that for the older HV2 fabricated Al-AlO_x-Al

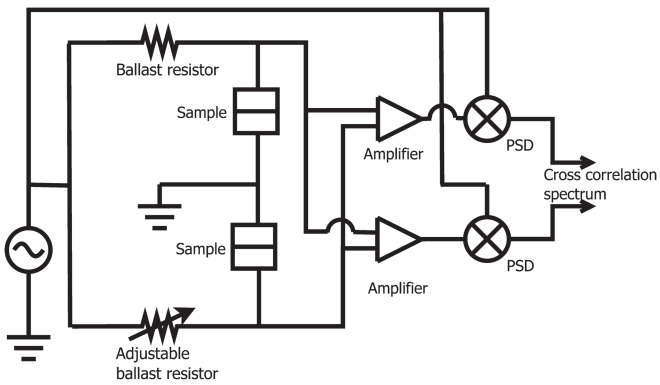

FIG. 4. Schematic of the AC modulation bridge noise measurement setup with two pre- and lock-in amplifiers (PSD) and a cross-correlation spectrum analyzer. The fixed ballast resistor has a resistance of 1 MΩ, and the adjustable resistor (General Radio 1433B) is used to balance the bridge. Due to the bridge measurement technique two tunnel junctions are measured together.

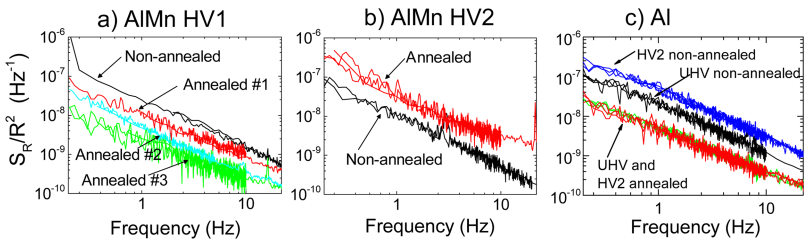

FIG. 5. Room temperature resistance noise spectral densities S_R of double Al:Mn-AlOx-Al (a and b) and Al-AlOx-Al (c) tunnel junsction samples fabricated in a) HV1, b) HV2 and c) UHV and HV2 evaporators before and after annealing.[13] The data is normalized with R_T^2. The measured scaled spectra were reproducible from sample to sample, except in the case b) where it was found that the noise levels in annealed samples varied.

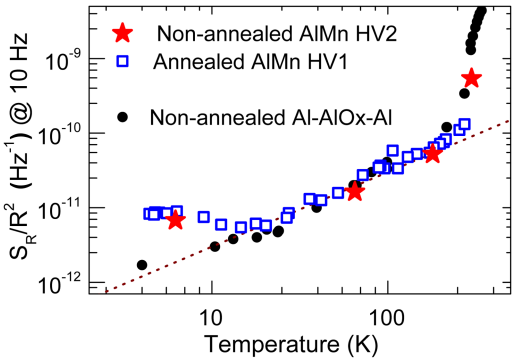

FIG. 6. Temperature dependence of the normalized $1/f$ resistance noise power density at 10 Hz in an annealed Al:Mn-AlOx-Al NIS junction made in HV1 (squares), and in a similar non-annealed junction made in HV2 (stars). Old data[13] of non-annealed Al-AlOx-Al tunnel junctions made in UHV is also shown. The dotted line shows a linear temperature dependence $3 \cdot 10^{-13} T$ 1/Hz. The temperature dependence in all samples coincides, except at the very lowest temperatures where NIS junctions have higher noise levels than Al-AlOx-Al junctions.

junctions the noise level is somewhat higher than for the HV2 fabricated Al:Mn-AlO_x-Al junctions. Strong conclusions are hard to draw, however, as there is a significant time difference between the old and the new measurements, during which the quality of the evaporator could have changed (for the better in this case).

After annealing, the level of $1/f$ noise clearly diminished in the Al:Mn-AlO_x-Al samples made in the "cleaner" HV1 evaporator, in the best case by an order of magnitude [Annealed #3 in Fig. 5(a)], consistent with the earlier results with Al-AlO_x-Al junctions, Fig. 5(c).[13] The obtained noise level for sample Annealed #3 was even below the annealed noise in Al-AlO_x-Al junctions. However, this level of reduction was not reproducible between different samples, but varied up to a factor of five, as shown by the examples in Fig. 5(a). On the other hand, the $1/f$ noise in all Al:Mn-AlO_x-Al junctions made in evaporator HV2 *increased* after annealing. This discrepancy between the results of HV1 and HV2 is quite surprising, although we did see clear differences in aging and the level of rise of R_T between the samples made in HV1 and HV2. Note that in Al-AlO_x-Al junctions, we never saw an increase with annealing. Thus, the manganese content and its changes with annealing is a likely factor for the increase.

For two samples, the $1/f$ noise was measured also from room temperature down to 4.2 K, as shown in Fig. 6, one annealed HV1 sample [Annealed #2 in Fig. 5(a)], and one non-annealed HV2 sample. The same kind of temperature dependence is seen for both junctions, and that temperature dependence mostly coincides with the one measured for Al-AlOx-Al junctions, also shown in Fig. 6. At intermediate temperatures between 10 K and 200 K, the temperature dependence is linear in agreement with previous work with Al-AlOx-Al junctions.[12,15] At high temperatures above ~ 200 K, there is a strong increase in the temperature dependence, which is also seen in Al-AlO_x-Al junctions. On the other hand, at temperatures below 10 K, an interesting increase/saturation in the noise level in both Al:Mn-AlO_x-Al NIS junctions is observed, in contrast to the Al-AlO_x-Al results. More work is required to understand if this is universal and what could possibly cause it.

VI. ELEMENTAL ANALYSIS

Finally, accelerator based material analysis was performed to "see" inside the films, to gain insight on the effects of annealing and the measured electrical differences between the different evaporators. Time-of-Flight Elastic Recoil Detection Analysis (ToF-ERDA), a method for elemental depth profile analysis,[51] was performed for larger area test samples (direct probing of micron-scale devices is not currently possible with the ToF-ERDA technique), using a 7.765 MeV 35Cl beam from a Pelletron accelerator. Both the energy and the time-of-flight of recoiled atoms were measured accurately, allowing plotting of the depth profile of different masses individually.[51] The depth resolution, is in the nanoscale with ToF-ERDA, in these measurements around ~ 5 nm, and the

elemental sensitivity is below 1 atomic %. However, even with such an impressive depth resolution, we cannot hope to resolve the actual tunneling barrier regions, which are typically 1-2 nm thick.[7,43]

The test samples were fabricated using the same materials (Al:Mn and Al) and protocols as for the sub-micron junctions, with the exception that no lithography was performed. Non-annealed and annealed samples were fabricated in the same exact evaporation runs for both evaporators HV1 and HV2. Thus, any changes in elemental profiles result from the annealing, and not from variations of evaporation conditions. Due to the possible modification of samples due to ion irradiation during the ToF-ERDA measurements, it is not possible to measure the same sample twice, both before and after annealing.

In Fig. 7, we first plot the depth profiles for aluminum and manganese, for samples fabricated in evaporators HV1 and HV2, both before and after annealing. The aluminum concentration and profile is quite similar for all samples. In contrast, in the manganese concentration, a clear difference is seen before and after annealing for the HV2 sample, where initially a non-uniform manganese profile was observed, with more manganese deeper in the film (earlier during evaporation). With annealing, some manganese clearly moves away from the vicinity of the Al:Mn/Al interface where the tunneling barrier is located, more towards the surface. No such changes are seen for the sample HV1, where the manganese profile is uniform initially.

Another point to notice is that the measured concentration for manganese is around 10 at. %, slightly different between HV1 and HV2 evaporations, and much larger than the concentration of the source at 2 at. %. This agrees with previous work,[35] where an increase in Mn concentration in e-beam evaporation was also reported and attributed to the large vapor pressure differences between Al and Mn. The differences between the Al:Mn films fabricated in the two evaporators can perhaps be attributed to a difference in the evaporators' control of the electron beam: In HV1, the electron beam heating the metal in the crucible is swept, heating a larger area, whereas in HV2 the e-beam is stationary leading to a smaller hot spot. It seems that such stationary electron beam distorts the manganese concentration in the source more severely, leading to changes in the manganese evaporation rate during deposition.

The changes in manganese concentration near the barrier observed in the HV2 samples could perhaps explain the puzzling increase of the $1/f$ noise after annealing in the sub-micron HV2 samples. We hypothesize that the observed diffusion of Mn away from the junction area may create more charge traps at the tunnel barrier interface, leading to increased $1/f$ noise. In HV1 samples this reorganization does not take place as the profile is more uniform, and thus the noise can actually decrease due to the reduction of the traps inside the barrier.

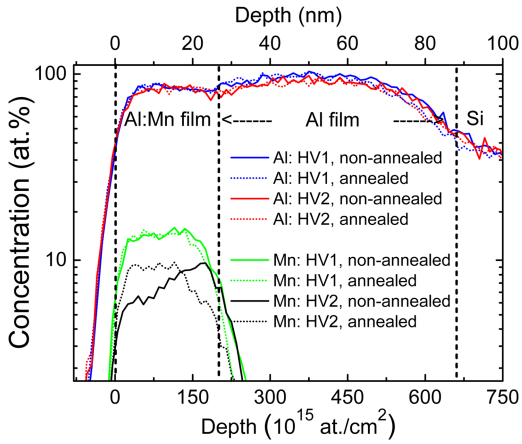

FIG. 7. ToF-ERDA depth profile measurement data showing both aluminium and manganese concentrations as function of the film depth, shown for both annealed (dashed) and non-annealed (solid) samples made in evaporators HV1 and HV2. The dashed vertical lines show the approximate positions of the surfaces and interfaces. For HV2, the non-uniform manganese profile changes in annealing.

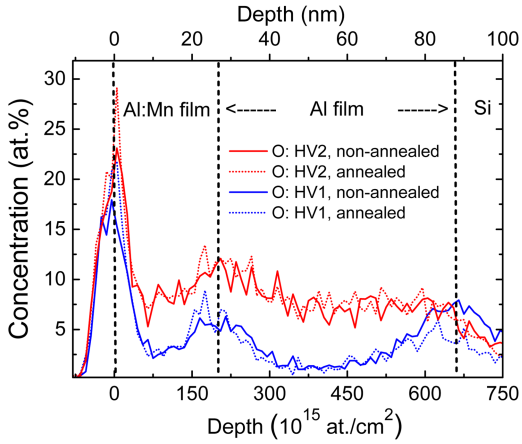

FIG. 8. ToF-ERDA depth profile measurement data showing oxygen content as a function of the film depth. The largest peak is the surface oxidation. The tunneling barrier oxide is located approximately at 30 nm from the surface.

We also discuss the elemental profiling results of the impurity elements oxygen, carbon and hydrogen, shown in Figs. 8 –10. These elements are essentially always present, but in our case we of course expect to see large oxygen concentrations on the surface of the Al:Mn film due to exposure to room air, and at the Al:Mn-Al interface due to the controlled *in-situ* oxidation of the tunneling barrier.

The oxygen profiles shown in Fig. 8 seem initially somewhat surprising. Although the surface oxide layer is clearly visible in all samples, the buried oxide at the Al:Mn/Al interface is much less so. The thickness of the two oxide layers should not be much different, as room temperature Al thermal oxidation is self-limiting.[52] However, the difference can most likely be be attributed to chemisorbed water and OH groups on the surface of the sample.[53] Another visible feature is the clearly non-zero and higher oxygen concentrations through the Al:Mn and Al films in samples fabricated in HV2, the more "dirty" evaporator. Apparently, Al films with oxygen concentration around 7 at. % (deep inside the Al film) remain easily metallic. The oxygen content does not seem to change significantly during annealing, although some increase at the surface is visible, resulting perhaps from an uncontrolled high temperature (400 °C) thermal oxidation in the annealing vacuum chamber.

The concentration of carbon and hydrogen impurities is plotted in figures 9 and 10. Carbon profiles are quite similar in all samples, with noticeable surface contaminations, and no clear profile changes with the annealing. Largest amounts of hydrogen are seen at the surface and also penetrating

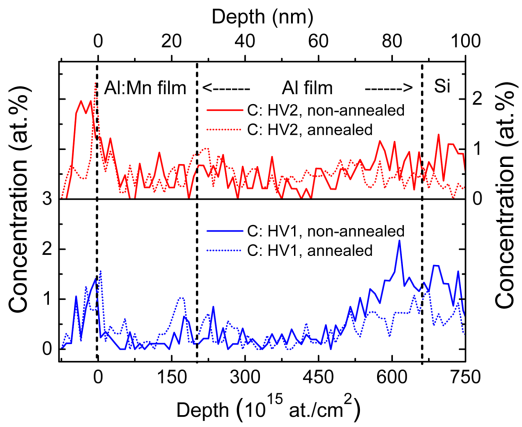

FIG. 9. ToF-ERDA depth profile measurement data showing carbon concentration as a function of the film depth. There is no difference in amount of carbon between the two evaporators, but reduction of 16% in HV2 and 25% in HV1 samples was seen after annealing.

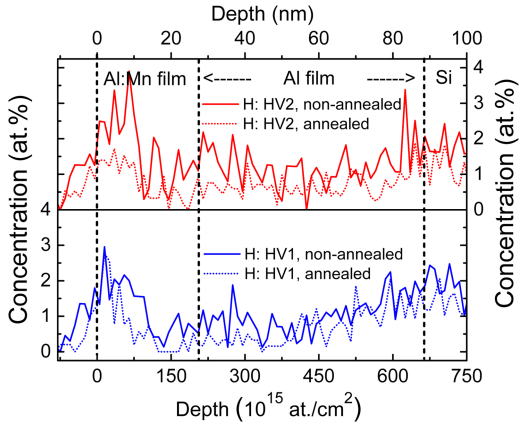

FIG. 10. ToF-ERDA depth profile measurement data showing hydrogen concentration as a function of the film depth. There is 15% more hydrogen in non-annealed HV2 sample than in non-annealed HV1 sample. Also a reduction of 29% in HV1 sample and 42% in HV2 sample in hydrogen amount is seen after annealing.

into the Al:Mn films a bit. The initial hydrogen content of the HV2 films are higher, and annealing reduces the amount of hydrogen impurities quite clearly by 30 - 40 %. As most of the C and H contamination is seen outside the tunnel barrier region, it is unlikely that they contribute to the junction $1/f$ noise or sub-gap current.

VII. CONCLUSIONS

We have studied the effects of vacuum annealing on the properties of NIS junctions made using various normal metal electrodes (Cu,Au,Ag,AuPd, Al:Mn), Al as the superconductor, and thermally oxidized AlO_x as the tunneling barrier. Only Al:Mn, aluminum-manganese alloy, produced good junctions after annealing. The tunneling resistance of the Al:Mn-AlO_x-Al junctions increased after annealing, typically by factors 2-5, and the stability of the junctions was much improved, as seen by the significant reduction of long-term drift (aging). These results are in general agreement with earlier annealing work for Al-AlO_x-Al junctions.[7]

The measurements on the current-voltage characteristics at sub-Kelvin temperatures revealed that the annealing had no negative effects on the junction characteristics. Specifically, the superconducting gap stayed constant, and the sub-gap current scaled down the same way as the above-the-gap current with the increase of the tunneling resistance R_T, as $I \sim 1/R_T$. This is expected if the sub-gap current is dominated by single-particle tunneling. In principle, annealing is expected to lower the two-particle Andreev tunneling much more, which could benefit the performance of metrological SINIS turnstiles and SINIS tunnel junction coolers.

The low-frequency $1/f$ resistance noise of the Al:Mn-AlO_x-Al junctions was also studied. Annealing reduced the observed noise, in best cases by over an order of magnitude, reaching levels even below annealed Al-AlO_x-Al junctions. However, the reduction was variable from sample to sample, and for some devices even increase of noise was observed. The temperature dependence followed trends seen for Al-AlO_x-Al junctions,[13] in particular linear temperature dependence of the noise spectral density was seen between 10 K - 200 K, with a similar noise level. All indications point to the conclusion that the $1/f$ noise in both junction types is generated mostly by the same mechanism, typically attributed to charge traps in or near the barrier,[19] and the linear temperature dependence is in agreement with other recent experiments in sub-micron Al-AlO_x-Al junctions[12,15] and with the simplest theories of fluctuating charge traps.[11]

Furthermore, accelerator-based material analysis was used to probe the material concentration profiles of the films. After annealing, changes in the manganese concentration profile (diffusion) near the tunnel junction were observed, if the initial profile was non-uniform. These changes were observed in samples which were fabricated the same way as the samples where $1/f$ noise increased

after annealing. Thus, we speculate that the two phenomena may be correlated. Annealing also reduced the overall amount of hydrogen impurities in the films, but not of oxygen.

ACKNOWLEDGMENTS

This study was supported by the Academy of Finland project number 260880 and the Finnish Cultural Foundation.

[1] J. Clarke and F. K. Wilhelm, Nature **453**, 1031 (2008).
[2] J. P. Pekola, O.-P. Saira, V. F. Maisi, A. Kemppinen, M. Möttönen, Y. A. Pashkin, and D. V. Averin, Rev. Mod. Phys. **85**, 1421 (2013).
[3] J. T. Muhonen, M. Meschke, and J. P. Pekola, Reports on Progress in Physics **75**, 046501 (2012).
[4] P. Lerch and A. Zehnder, *Cryogenic Particle Detection*, edited by C. Enss, Topics in Applied Physics (Springer, Berlin, 2005) p. 217.
[5] F. Giazotto, T. T. Heikkilä, A. Luukanen, A. M. Savin, and J. P. Pekola, Rev. Mod. Phys. **78**, 217 (2006).
[6] H. Grabert and M. H. Devoret, *Single Charge Tunneling, Coulomb Blockade Phenomena In Nanostructures* (Plenum Press, New York, 1992).
[7] P. J. Koppinen, L. M. Väistö, and I. J. Maasilta, Applied Physics Letters **90**, 053503 (2007).
[8] I. M. Pop, T. Fournier, T. Crozes, F. Lecocq, I. Matei, B. Pannetier, O. Buisson, and W. Guichard, Journal of Vacuum Science & Technology B **30**, 010607 (2012).
[9] T. Holmqvist, M. Meschke, and J. P. Pekola, Journal of Vacuum Science & Technology B **26**, 28 (2008).
[10] M. B. Weissman, Rev. Mod. Phys. **60**, 537 (1988).
[11] P. Dutta and P. M. Horn, Rev. Mod. Phys. **53**, 497 (1981).
[12] C. D. Nugroho, V. Orlyanchik, and D. J. Van Harlingen, Applied Physics Letters **102**, 142602 (2013).
[13] J. K. Julin, P. J. Koppinen, and I. J. Maasilta, Applied Physics Letters **97**, 152501 (2010).
[14] S. Pottorf, V. Patel, and J. E. Lukens, Applied Physics Letters **94**, 043501 (2009).
[15] J. Eroms, L. C. van Schaarenburg, E. F. C. Driessen, J. H. Plantenberg, C. M. Huizinga, R. N. Schouten, A. H. Verbruggen, C. J. P. M. Harmans, and J. E. Mooij, Applied Physics Letters **89**, 122516 (2006).
[16] D. J. Van Harlingen, T. L. Robertson, B. L. T. Plourde, P. A. Reichardt, T. A. Crane, and J. Clarke, Phys. Rev. B **70**, 064517 (2004).
[17] F. C. Wellstood, C. Urbina, and J. Clarke, Applied Physics Letters **85**, 5296 (2004).
[18] B. Savo, F. C. Wellstood, and J. Clarke, Applied Physics Letters **50**, 1757 (1987).
[19] C. T. Rogers and R. A. Buhrman, Phys. Rev. Lett. **53**, 1272 (1984).
[20] M. Constantin and C. C. Yu, Phys. Rev. Lett. **99**, 207001 (2007).
[21] G. Zimmerli, T. M. Eiles, R. L. Kautz, and J. M. Martinis, Applied Physics Letters **61**, 237 (1992).
[22] A. B. Zorin, F.-J. Ahlers, J. Niemeyer, T. Weimann, H. Wolf, V. A. Krupenin, and S. V. Lotkhov, Phys. Rev. B **53**, 13682 (1996).
[23] O. Astafiev, Y. A. Pashkin, Y. Nakamura, T. Yamamoto, and J. S. Tsai, Phys. Rev. Lett. **96**, 137001 (2006).
[24] S. Kafanov, H. Brenning, T. Duty, and P. Delsing, Phys. Rev. B **78**, 125411 (2008).
[25] M. V. Gustafsson, A. Pourkabirian, G. Johansson, J. Clarke, and P. Delsing, Phys. Rev. B **88**, 245410 (2013).
[26] J. P. Pekola, J. J. Vartiainen, M. Möttönen, O.-P. Saira, M. Meschke, and D. V. Averin, Nature Physics **4**, 120 (2008).
[27] M. Nahum and J. M. Martinis, Appl. Phys. Lett. **63**, 3075 (1993).
[28] D. R. Schmidt, K. W. Lehnert, A. M. Clark, W. D. Duncan, K. D. Irwin, N. Miller, and J. N. Ullom, Applied Physics Letters **86**, 053505 (2005).
[29] S. Gasparinetti, K. L. Viisanen, O.-P. Saira, T. Faivre, M. Arzeo, M. Meschke, and J. P. Pekola, Phys. Rev. Applied **3**, 014007 (2015).
[30] J. P. Pekola, T. T. Heikkilä, A. M. Savin, J. T. Flyktman, F. Giazotto, and F. W. J. Hekking, Phys. Rev. Lett. **92**, 056804 (2004).
[31] S. Chaudhuri and I. J. Maasilta, Applied Physics Letters **104**, 122601 (2014).
[32] R. C. Dynes, J. P. Garno, G. B. Hertel, and T. P. Orlando, Phys. Rev. Lett. **53**, 2437 (1984).
[33] S. T. Ruggiero, A. Williams, W. H. Rippard, A. Clark, S. W. Deiker, L. R. Vale, and J. N. Ullom, Journal of Low Temperature Physics **134**, 973 (2004).
[34] A. M. Clark, A. Williams, S. T. Ruggiero, M. L. van den Berg, and J. N. Ullom, Applied Physics Letters **84**, 625 (2004).
[35] L. J. Taskinen and I. J. Maasilta, Applied Physics Letters **89**, 143511 (2006).
[36] M. J. Martinez-Perez and F. Giazotto, Nature Communications **5**, 3579 (2014).
[37] P. J. Koppinen and I. J. Maasilta, Phys. Rev. Lett. **102**, 165502 (2009).
[38] J. P. Pekola, V. F. Maisi, S. Kafanov, N. Chekurov, A. Kemppinen, Y. A. Pashkin, O.-P. Saira, M. Möttönen, and J. S. Tsai, Phys. Rev. Lett. **105**, 026803 (2010).
[39] S. Rajauria, P. Gandit, T. Fournier, F. W. J. Hekking, B. Pannetier, and H. Courtois, Phys. Rev. Lett. **100**, 207002 (2008).
[40] T. Greibe, M. P. V. Stenberg, C. M. Wilson, T. Bauch, V. S. Shumeiko, and P. Delsing, Phys. Rev. Lett. **106**, 097001 (2011).
[41] F. W. J. Hekking and Y. V. Nazarov, Phys. Rev. B **49**, 6847 (1994).
[42] J. S. Bae, K. H. Shin, T. D. Lee, and H. M. Lee, Applied Physics Letters **80**, 1168 (2002).
[43] T. Aref, A. Averin, S. van Dijken, A. Ferring, M. Koberidze, V. F. Maisi, H. Q. Nguyend, R. M. Nieminen, J. P. Pekola, and L. D. Yao, Journal of Applied Physics **116**, 073702 (2014).
[44] R. Barends, J. Wenner, M. Lenander, Y. Chen, R. C. Bialczak, J. Kelly, E. Lucero, P. OMalley, M. Mariantoni, D. Sank, H. Wang, T. C. White, Y. Yin, J. Zhao, A. N. Cleland, J. M. Martinis, and J. J. A. Baselmans, Applied Physics Letters **99**, 113507 (2011).

[45] A. D. Corcoles, J. M. Chow, J. M. Gambetta, C. Rigetti, J. R. Rozen, G. A. Keefe, M. Beth Rothwell, M. B. Ketchen, and M. Steffen, Applied Physics Letters **99**, 181906 (2011).
[46] O.-P. Saira, A. Kemppinen, V. F. Maisi, and J. P. Pekola, Phys. Rev. B **85**, 012504 (2012).
[47] A. Kemppinen, S. V. Lotkhov, O.-P. Saira, A. B. Zorin, J. P. Pekola, and A. J. Manninen, Applied Physics Letters **99**, 142106 (2011).
[48] F. W. J. Hekking and Y. V. Nazarov, Phys. Rev. Lett. **71**, 1625 (1993).
[49] D. V. Averin and J. P. Pekola, Phys. Rev. Lett. **101**, 066801 (2008).
[50] J. H. Scofield, Rev. Sci. Instrum **58**, 985 (1987).
[51] M. Laitinen, M. Rossi, J. Julin, and T. Sajavaara, Nuclear Instruments and Methods in Physics Research Section B: Beam Interactions with Materials and Atoms **337**, 55 (2014).
[52] L. P. H. Jeurgens, W. G. Sloof, F. D. Tichelaar, and E. J. Mittemeijer, Journal of Applied Physics **92**, 1649 (2002).
[53] E. McCafferty and J. P. Wightman, Surface and Interface Analysis **26**, 549 (1998).